Journal of Solid State Chemistry 258 (2018) 488–494

Contents lists available at ScienceDirect

Journal of Solid State Chemistry

journal homepage: www.elsevier.com/locate/jssc

Role of organic cations on hybrid halide perovskite $CH_3NH_3PbI_3$ surfaces

Qiang Teng[a], Ting-Ting Shi[b], Ren-Yu Tian[a], Xiao-Bao Yang[a], Yu-Jun Zhao[a,b,*]

[a] Department of Physics, South China University of Technology, Guangzhou, Guangdong 510640, China
[b] School of Materials Science and Engineering, South China University of Technology, Guangzhou, Guangdong 510640, China

ARTICLE INFO

Keywords:
$CH_3NH_3PbI_3$ surface
Organic cation orientation
Structural stability
Electronic property

ABSTRACT

Organic-inorganic hybrid halide perovskite $CH_3NH_3PbI_3$ ($MAPbI_3$) has received rapid progress in power conversion efficiency as promising photovoltaic materials, yet the surface structures and the role of MA cations are not well understood. In this work, we investigated the structural stability and electronic properties of (001) surface of cubic, (001) and (110) surfaces of tetragonal and orthorhombic phases of $MAPbI_3$ with considering the *orientation* of MA cations, by density functional theory calculations. We demonstrate that the orientation of MA cations has profound consequences on the structural stability and the electronic properties of the surfaces, in contrast to the bulk phases. Compared with the MA-I terminated surfaces, the Pb-I_2 terminated ones generally have smaller band gaps and the advantage to enable the photo-excited holes to transfer to the hole-transport materials in both tetragonal and orthorhombic phases. Overall, we suggest that the films with Pb-I_2 terminated surfaces would prevail in high performance solar energy absorbers.

1. Introduction

Organic-Inorganic hybrid halide perovskite solar cells (PSCs), such as $CH_3NH_3PbX_3$ (X = I, Cl, Br), have attracted much interest because of their enormous potential as low-cost and high performance photovoltaic materials. Since the $MAPbI_3$ material was first used as dye-sensitized solar cells by Miyasaka et al. [1] in 2009, the power conversion efficiencies (PCEs) of the PSCs have been rapidly increasing from 3.8% to a current confirmed 22.1% [2–16], approaching to those of GaAs and crystalline silicon thin film solar cells [17]. Such rapid progress is unprecedented in the solar energy arena, and thus PSCs are considered as the most competitive candidates for the next generation solar cells. Their outstanding photovoltaic performance is mainly attributed to the unique properties, such as high absorption, long carrier lifetimes and larger diffusion lengths observed in PSCs [9,18–24].

It is known that perovskites with formula ABX_3 can adapt various crystal structures depending on the relative sizes and the interaction between the cation A and the corner-sharing BX_6 octahedral, with a reasonable prediction of the preferable structure from the empirical Goldschmidt tolerance factor t [25]. For perovskite, with formula ABX_3, t is given by the ionic radius of the atoms in the form:

$$t = \frac{R_A + R_X}{\sqrt{2}(R_B + R_X)},$$

where R_A, R_B, and R_X are the ionic radius of corresponding ions. In general, halide perovskite structures may prevail when t lies in the range of 0.81–1.11 [26], and a cubic structure with a tolerance factor of 0.9–1.0 [25]. Smaller t could result in distorted tetragonal or orthorhombic structures with tilted octahedral. For a large cation A, t could be greater than one, leading to a layered hybrid perovskite structure as the three-dimensional (3D) B-X network is destabilized [25,27,28]. Actually, most perovskite materials experience transitions among the above structures at specific temperatures. For $MAPbI_3$, the cubic to tetragonal and consequently to orthorhombic phase transitions occur at about 330 K and 160 K, respectively [29]. Even though the phases of $MAPbI_3$ are available at different temperature, there are chances for films with the various phases appear in devices due to constrain from substrates or other factors. For instance, cubic and orthorhombic phases were investigated experimentally [30,31].

Surfaces and interfaces are always involved in practical devices. Typically, PSCs are layered structures, which are assembled by the electron-transport layer, perovskite light absorber and hole-transport layer [1,32]. Accordingly, the properties of surface and interface as well as charge transport layers [33] are considered to play a crucial role in carrier transportation and recombination, and thus the ultimate performance of PSCs. In particular, the orientation of organic cations cannot be ignored. Even if MA orientation distributes randomly in the bulk, the order might be introduced when polarized molecules are adsorbed, or intrinsic polarization is possessed on substrates.

Recently, experimental and theoretical studies revealed an important role of organic cations in determining the structural, electronic, and optical properties of organic-inorganic halide perovskites [34–38].

* Corresponding author at: Department of Physics, South China University of Technology, Guangzhou, Guangdong 510640, China.
E-mail address: zhaoyj@scut.edu.cn (Y.-J. Zhao).

https://doi.org/10.1016/j.jssc.2017.10.029
Received 25 July 2017; Received in revised form 20 October 2017; Accepted 22 October 2017
Available online 23 October 2017

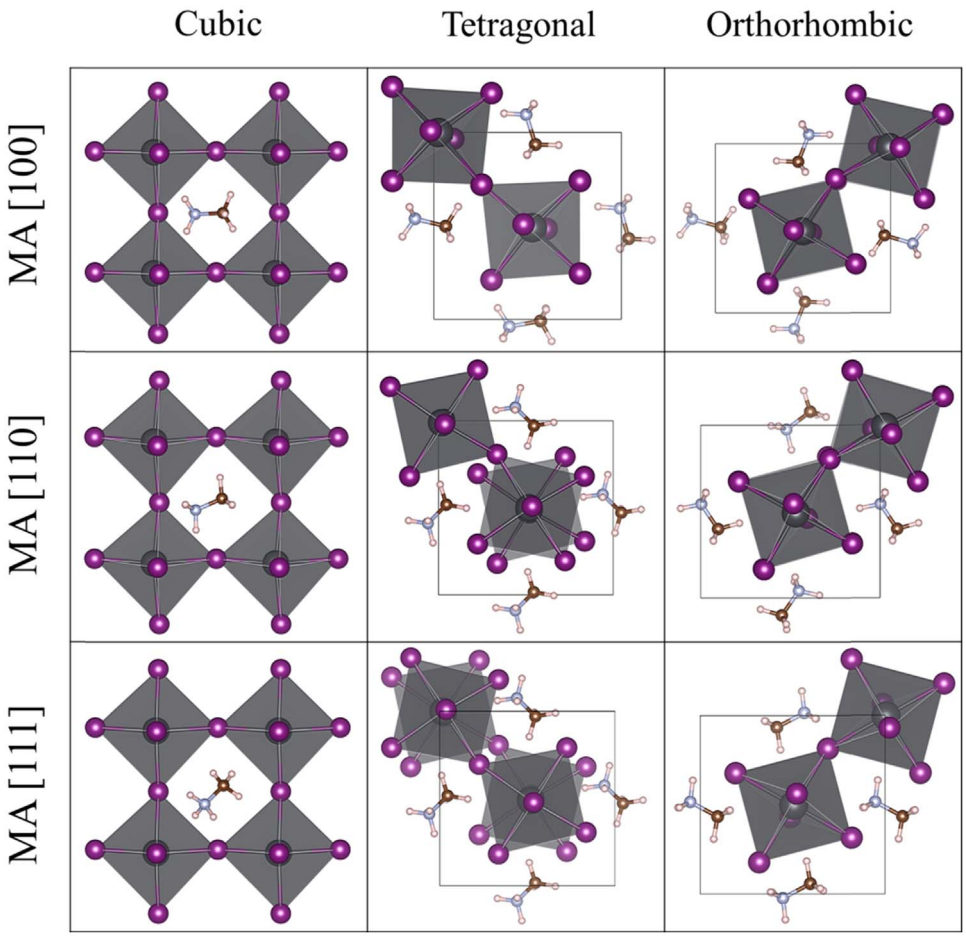

Fig. 1. Optimized stable structures [top view from (001) direction] of the cubic, tetragonal and orthorhombic phases of $MAPbI_3$ for three different orientations of MA cations.

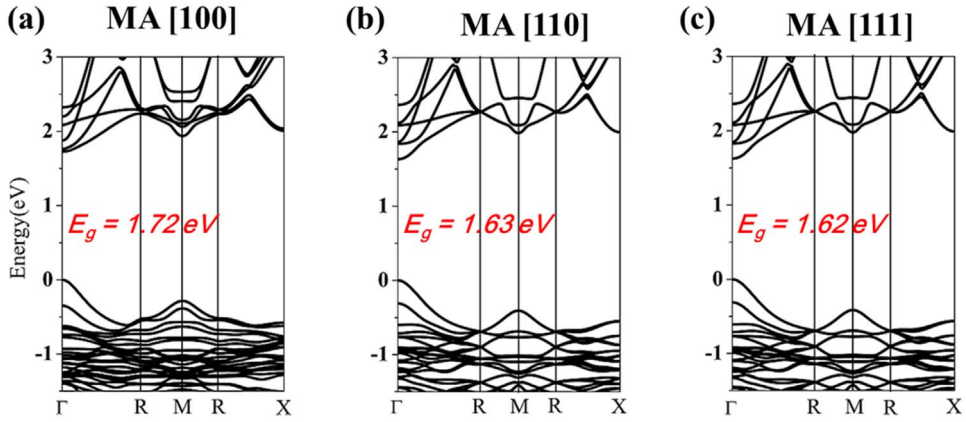

Fig. 2. Calculated band structures of the tetragonal phase of $MAPbI_3$ bulk $MAPbI_3$ for three different orientations of MA cations: (a) [100], (b) [110], and (c) [111] directions.

Although the role of the orientation of MA on bulk $MAPbI_3$ has been substantially studied by first-principles calculations and the results reveal the orientation of MA cations has effect on the electronic structures [37,39,40], they have not been systematically studied on surfaces so far. Even in other works involved the surface stability, the effects of MA orientation were not considered, which the MA orientation is often fixed to keep the polarization cancelled [41–44]. The fundamental mechanisms regarding whether the orientation of MA cations can influence the structural stability and the electronic properties of surface is still unclear. Thus, there are great interests in providing a clear understanding of how the behavior of the orientation of the MA cations affects the structural stability and electronic properties of surfaces of $MAPbI_3$.

In this study, the structural stability and electronic properties of (100) surface of cubic, (001) and (110) surfaces of tetragonal and orthorhombic phases of $MAPbI_3$ with consideration the orientations of MA cations, were systematically investigated by density functional theory (DFT) calculations, respectively. We find that the structural stability and the electronic properties of surfaces for *cubic*, *tetragonal* and *orthorhombic* phases clearly depend on the orientation of the MA cations. In addition, compared with the MA-I terminations, the Pb-I_2 terminations have smaller band gaps and can better transfer the photoexcited holes to the adjacent hole transport materials (HTMs) with smaller energy loss.

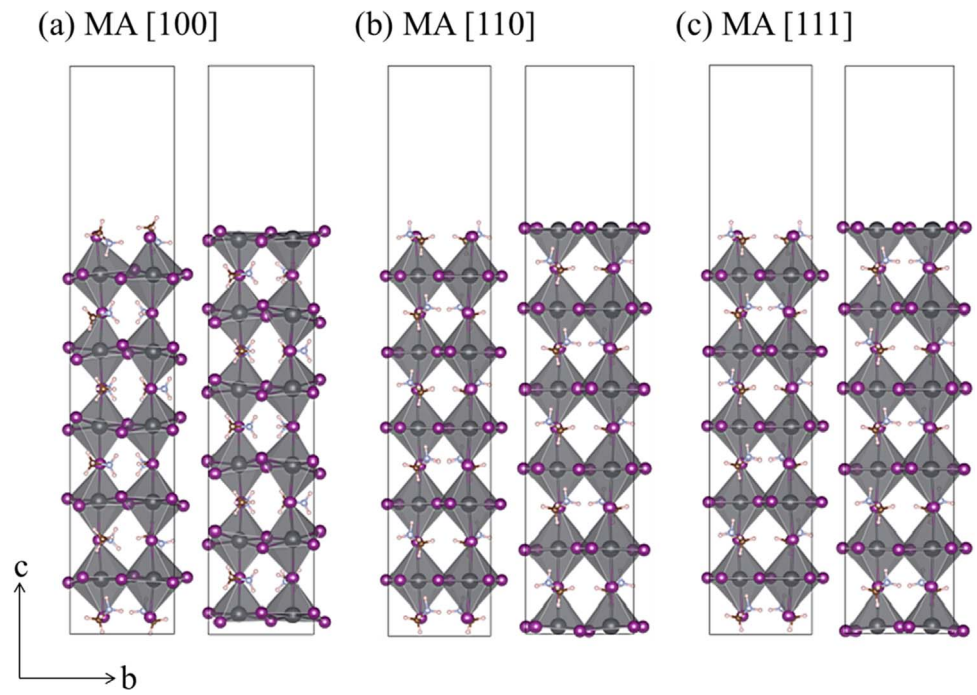

Fig. 3. Relaxed surface terminations on (001) surfaces of tetragonal phase with MA cations along (a) [100], (b) [110] and (c) [111] directions. The left and right structures indicate a stable MAI and PbI_2 terminations, respectively (small white: hydrogen; small brown: carbon; small silver: nitrogen; dark gray: lead; purple: iodine). (For interpretation of the references to color in this figure legend, the reader is referred to the web version of this article)

2. Computational details

In this work, all the calculations were performed with DFT as implemented in Vienna Ab initio Simulation Package (VASP) [45,46]. The projector-augmented wave (PAW) method was used to describe the ion-electron interactions [47,48]. The valence configurations of 5*d*6*s*6*p* for Pb, 5*s*5*p* for I, 2*s*2*p* for C, 2*s*2*p* for N, and 1*s* for H were considered. The exchange-correlation was obtained approximately by generalized gradient approximation (GGA) with Perdew-Burke-Ernzerhof (PBE) formulism [49]. The nonlocal van der Waals (vdW) functional method as implemented in VASP [50] was adopted, as demonstrated properly for the system in earlier work by Tateyama et al. [41]. The cutoff energy of the plane wave basis was set to be 450 eV. The k-point grids of 5×5×5 and 5×5×1 Γ -centered were used for sampling the Brillouin zones of investigated bulk and surface for both orthorhombic and tetragonal phases, respectively. In the case of cubic phase, the 6×6×6 and 6×6×1 Γ -centered were used correspondingly.

The lattice parameters were fixed to the experimental values, namely, $a = b = c = 6.33$ Å for cubic phase; $a = b = 8.86$ Å and $c = 12.67$ Å for tetragonal phase; $a = 8.86$ Å, $b = 8.58$ Å and $c = 12.62$ Å for orthorhombic phase [51]. We started the geometrical optimization with the MA cations oriented along the [100, 110] and [111] directions. The atomic positions were fully relaxed until the residual force (Hellmann-Feynman forces) on each atom was less than 0.01 eV/Å in all investigated structures.

Based on the optimized bulk structures, we constructed slab models, including the (100) surfaces for cubic , the (110) and (001) surfaces for tetragonal and orthorhombic phases, respectively. To avoid the effect of the dipole and the thickness-dependent divergent surface energy [52], we constructed the slab with odd atomic layers, where the outermost layers are symmetrically equivalent save the MA cations orientations. A sufficient slab thickness is necessary to maintain the bulk electronic properties in the central layer of a slab. The surface energies are converged within 0.002 J m^{-2} when the slab thickness changes from 9 atomic layers to 11 atomic layers, indicating that an 11-at.-layer slab is proper for the surface stability study and adopted in this work. A vacuum region of 15 Å was adopted to minimize the spurious interaction between periodic slabs.

To compare the stability of different surfaces at various chemical conditions, we used the surface grand potential (SGP, Ω) method, which is widely used to evaluate the structural stability of surfaces [41,53–56]. The SGP per unit cell area is defined as

$$\Omega = \frac{1}{2S}[E_{slab} - \alpha(E_{MA}^{bulk} + \Delta\mu_{MA}) - \beta(E_{Pb}^{bulk} + \Delta\mu_{Pb}) - \gamma(E_{I_2}^{gas} + \Delta\mu_{I}), \quad (1)$$

where E_{slab} is the total energy of a relaxed slab; and S represents the surface area per unit cell; α, β, and γ are the numbers of MA, Pb, and I atoms in the slabs, respectively. $\Delta\mu_{MA}$, and $\Delta\mu_{Pb}$, represent the relative chemical potentials of the MA cation and Pb to their respective bulk phases, while $\Delta\mu_I$ is with respect to molecule I_2.

Under the thermodynamic equilibrium growth conditions, the existence of $MAPbI_3$ satisfies [57]:

$$\Delta\mu_{MA} + \Delta\mu_{Pb} + 3\Delta\mu_{I} = \Delta H(MAPbI_3) \quad (2)$$

In order to avoid the formation of possible secondary phases PbI_2 and MAI, the following boundary conditions are required:

$$\Delta\mu_{MA} + \Delta\mu_{I} \leq \Delta H(MAI) \quad (3)$$

$$\Delta\mu_{Pb} + 2\Delta\mu_{I} \leq \Delta H(PbI_2) \quad (4)$$

$\Delta H(MAPbI_3)$, $\Delta H(MAI)$ and $\Delta H(PbI_2)$ are the formation enthalpies of $MAPbI_3$, MAI and PbI_2, respectively.

Furthermore, if the SGP is negative, the surface will form spontaneously and the corresponding crystal may not exist [53]. Therefore, to maintain the bulk crystal, the SGP is bounded to be positive and the following constraints should be considered [53]:

$$\Omega^i(\Delta\mu_{MA}, \Delta\mu_{Pb}, \Delta\mu_{I}) = 0, \quad (5)$$

where i refers to the surface corresponding lowest SGP.

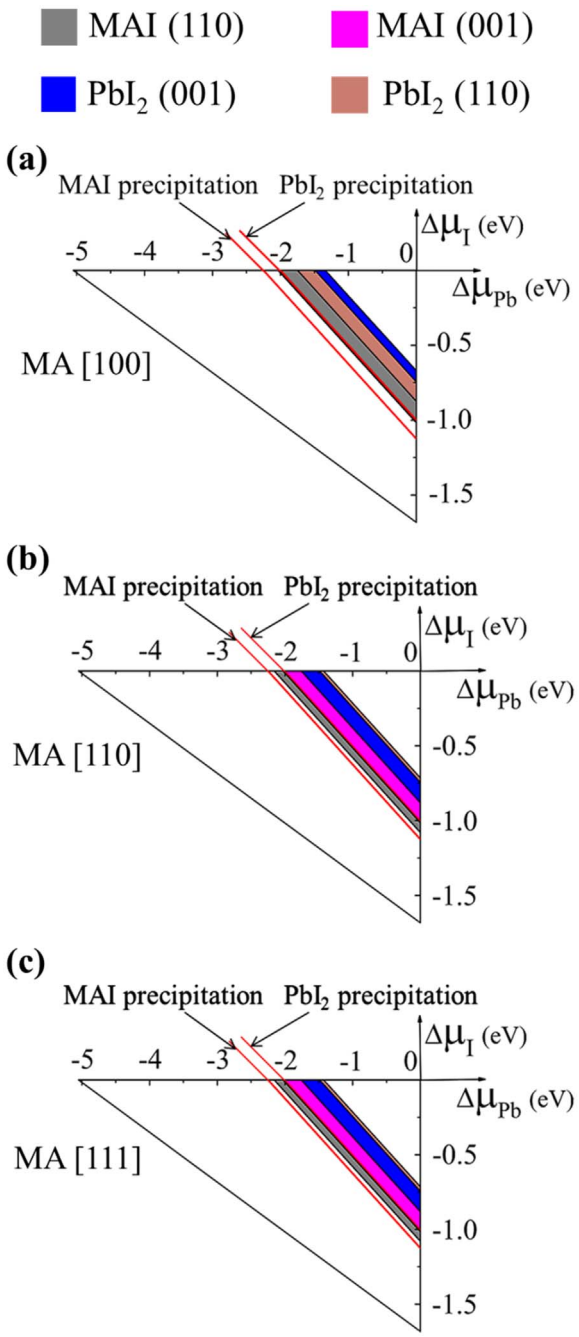

Fig. 4. The (001) and (110) surfaces termination stability diagram of tetragonal phase with three different orientations of MA cations, namely along (a) [100], (b) [110] and (c) [111], respectively.

3. Results and discussion

3.1. Bulk properties

The noncentrosymmetric organic cation MA has many possible orientations, and thus the atomic structures of $MAPbI_3$ are more complicate than those of inorganic perovskites. We have relaxed the cubic, tetragonal and orthorhombic phases of $MAPbI_3$ with the MA cations initially oriented along the [100, 110] and [111] directions. The optimized $MAPbI_3$ for different orientations of MA cations are shown in Fig. 1. Interestingly, the orientation of MA cations automatically ended up with MA cations along [110] in the orthorhombic phase after structure optimization while initially at [111] direction. Nevertheless, the energy difference for different MA orientations among the same phase is small, about 0.02 eV/f.u in both cubic and tetragonal, and 0.05 eV/f.u in orthorhombic phases, respectively. This may lead to the fact that the orientation of MA cations in $MAPbI_3$ is often disordered in experimental observation [58]. The chemical potential range of Pb and I satisfying Eqs. (2)–(4) for bulk phases are shown as the red region in Fig. S1 in the Supporting information for different MA orientations, indicating that the equilibrium growth of $MAPbI_3$ can occur only in a narrow and long range of chemical potentials, in line with previous results [59]. It implies that the $MAPbI_3$ compounds can be easily decomposed into MAI and PbI_2 independent of the phases and MA orientations.

The calculated band structures of the tetragonal *bulk* $MAPbI_3$ are displayed in Fig. 2, indicating the band gap is slightly greater when MA cations is oriented along [100] direction. The band gaps from the PBE results match well with the previous experimental and theoretical results [1,39,42,60,61], and largely due to the well-known cancellation of errors from GGA and non-SOC [39,62]. However, compared with the calculated results with consideration of SOC effect, the electronic structures and the fact that the *s* orbital of Pb has strong *sp* anti-bonding coupling with *p* orbital of I will be not influenced with the absence of SOC effect [60,63]. Regarding the structural properties, it is known that SOC typically has an impact of ~meV to the total energy of the compounds, and therefore is often neglected in the structural stability studies. In addition, it was discussed that SOC has a negligible effect on the lead-halide bond lengths and lattice parameters of lead-halide perovskites [64]. Therefore, the DFT-GGA calculations are feasible to investigate the stability, and the valence band maximum (VBM) and the conduction band minimum (CBM) bond characteristics of $MAPbI_3$ systems.

3.2. Surface stability

The relaxed (001) surface structures of tetragonal phase with various orientations of MA cations are shown in Fig. 3, and the rest of surface structures are depicted in Fig. S4 in Supporting information. As illustrated in Fig. 3, the outermost layers were reconstructed by the rotation of the PbI_6 octahedron and organic cations. Compared with the inner layer, the NH_3 groups of MA cations in outmost layer would point inwards while the CH_3 groups point outwards. This may attribute to a stronger interaction between NH_3^+ and the inorganic part in the surface.

To explore the influence of the MA orientations on the structural stability to the surfaces, we calculated the SGP for all investigated surfaces. Here, based on Eqs. (2)–(4), the formation enthalpies of bulk $MAPbI_3$ can be calculated. Thus, the ranges of $\Delta\mu_I$ and $\Delta\mu_{Pb}$ were restricted for each investigated surface. Fig. 4 presents the stability diagram involving the surfaces of tetragonal phase, along with the range for bulk $MAPbI_3$. We note that, to form a pure surface (without considering the constrain from interface etc.), the corresponding termination region should be located on the thermodynamically stable range for the equilibrium of $MAPbI_3$. As shown in Fig. 4, the only region where a pure $MAPbI_3$ surface can be stabilized is restricted to the narrow stripe between the MAI precipitation line on the right and PbI_2 precipitation line on left.

As illustrated in Fig. 4, the orientation of MA cations has a profound impact on the stability of surfaces. When the MA cations oriented along the [100] direction, only the (110) surface of both terminations and the PbI_2 terminated (001) surface are available, but the region of the MAI-terminated (001) surface disappears in the stability diagram. Within the narrow strip, there is no stable surface with any termination, suggesting that the (001) and (110) surfaces of tetragonal phase could not be prepared under equilibrium or without considering constrains from substrate etc.

When MA oriented along [110] and [111] directions, all the investigated surfaces of tetragonal phase are available in the stability diagram. Furthermore, the MAI-terminated (110) surface region is

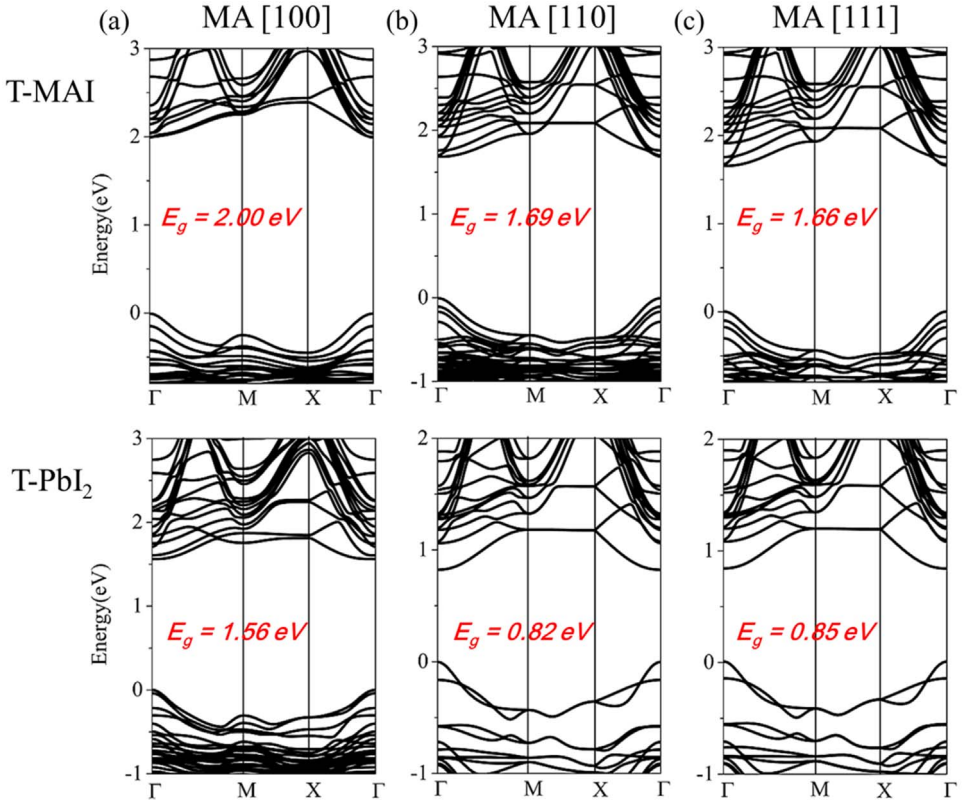

Fig. 5. Calculated band structures of (100) surface of tetragonal phase for the MA along: (a) [100], (b) [110], and (c) [111] directions. The up and down figures correspond to stable MAI and PbI_2 terminations, respectively.

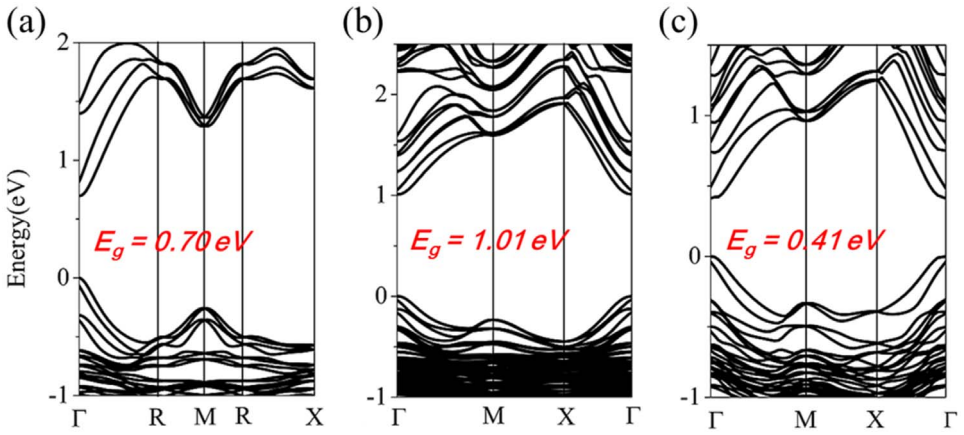

Fig. 6. Calculated band structures of the PbI_2 (a) and MAI (b) terminations of tetragonal phase, as well as the tetragonal bulk phase. Here the orientation of MA cations is all along [100] direction.

completely located in the narrow strip, implying the predominance of the termination in the tetragonal phase system. These differences may result from the fact that the orientations of MA cations greatly affect the interaction between the MA cations and the inorganic matrix, where the organic and the inorganic moieties play a vital role in determining the stability of organic-inorganic hybrid halide perovskites.

According to above discussion, significant interface effect is necessary to stabilize various terminated surfaces of the hybrid halide perovskites. Interestingly, some thin film surfaces were successfully prepared by experimentalists, as exemplified in Refs [65–67]. Accordingly, we would suggest experimentalists to prepare thin-film samples under Pb-rich and I-rich conditions, which favors the stability of PbI_2-terminated (110) surfaces, which prevails for hole transfer according to electronic structure analysis below. In addition, introducing polarization to the substrate surface, normal to the surface, will help stabilize the PbI_2-terminated (110) surface. The surface termination diagrams of cubic and tetragonal phases are illustrated in Fig. S5 of the Supporting information.

3.3. The electronic properties of surfaces

We now discuss the impact of orientation of MA cations on the electronic properties of surfaces. The calculated band structures of (001) and (110) surfaces of tetragonal phase for different orientations of MA cations are shown in Fig. 5. Clearly, the value of band gaps is significantly affected by the orientations of MA cations. The band gap of surfaces with the orientation of MA cations along [100] direction is generally greater than those along [110] and [111], suggesting that the interaction between the organic and the inorganic constituents has

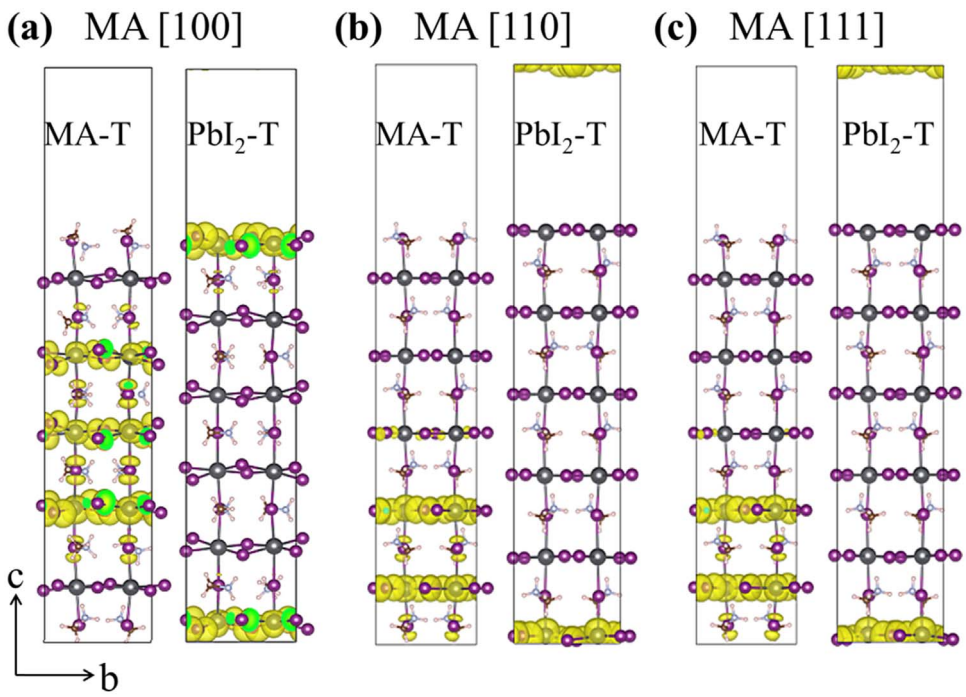

Fig. 7. Charge densities distribution of the VBM of (001) surface of tetragonal phase for three different orientations of MA cations: (a) [100], (b) [110], and (c) [111] directions.

significant impact on the structural properties, subsequently, which affects the electronic structure of the $MAPbI_3$ surfaces. The general dispersion of the bands is quite similar, showing that direct band gaps at the Γ point and no surface states in the band gap. These suggest that the electronic and optical properties of the surfaces should be similar to those of the bulk, and the hole-electron recombination will not occur dramatically at the surface, beneficial for realizing a long lifetimes and large diffusion length of the photo-excited carriers. Besides, compared with the PbI_2 terminations, the MAI terminations have larger band gaps, attributing to the larger distortion of [PbI_6] octahedral in MAI terminations than in the PbI_2 cases. It is well known that the octahedral distortion can substantially affect the band gap of halide perovskites [68]. The large octahedral distortion will reduce the bond angles of Pb-I-Pb, which weakens the overlap between the I *p* orbitals and the Pb *s* orbitals, resulting in a wider band gap [69]. Indeed, such feature can account for the difference of the band gap of the cubic, tetragonal and orthorhombic phase in lead halide perovskites and the larger band gap in Ge-based perovskites than the Sn and Pb cases. Interestingly, there is a discrepancy between the bulk phases and surfaces in their band gaps, where the band gaps of the MAI and PbI_2 terminations are larger and smaller than the bulk phase in $MAPbI_3$, respectively. This should be attributed to the limit of the slab size. It has been reported that the band gap of two dimensional lead-halide perovskites typically can be engineered by the layer thickness due to quantum confinement effects [70].

On the basis of our results and above discussions, we demonstrate that the MA orientation has effect on the stability and electronic properties of $MAPbI_3$ surfaces. Our calculated results are comparable with experimental results. Experimentally, Selig et al. recently reported that the orientation of MA cations may have effect on the electronic properties of the $MAPbX_3$ (X= I, Br, Cl) [71]. Subsequently, Kubicki et al. indicated that the organic cations reorientation can directly affect the performance of $MAPbI_3$ [72].

In addition, we have briefly examined the SOC effects for the electronic properties in the $MAPbI_3$. Fig. 6 shows the calculated band structures of the PbI_2 and MAI terminated of the (001) surface and the bulk phase with MA cations along [100] direction for tetragonal phase. Overall, no midgap state is formed in the energy window between the VBM and the CBM at the surfaces, in line with the absence of SOC solutions. Because of large SOC effect, the energies of the CBM are decreased about 1 eV in both surfaces and bulk of tetragonal phase in comparison with the without SOC solutions, whereas the energies of VBM are nearly unaffected, due to the Pb-6*p* character of conduction bands.

The charge density distribution of the VBM was also investigated for both the MAI and PbI_2 terminated of the (001) surfaces of tetragonal phase. As shown in Fig. 7, the charge density of VBM is mostly distributed in the inner layers of the surface for the MAI terminations, while they are localized at the outermost layer for the PbI_2 terminations. It should be noted that the surfaces with the charge density of the VBM localized at the outermost layers have the advantage over those distributed inside for transferring the photon induced holes to the adjacent HTMs. This implies that the PCEs of PbI_2 terminations will prevail over the MAI cases. Nevertheless, the orientation of the MA cations has little effect on the distribution of the charge density of the VBM in the surfaces of the tetragonal phase.

4. Conclusions

In summary, our study suggests that the orientation of MA greatly affects both the structural stability and the electronic properties of the surfaces, especially in contrast to the bulk cases.

i) Most ideal surfaces (without considering substrate effects) with different terminations are often instable with respect to the bulk $MAPbI_3$ under thermodynamic equilibrium, except MAI-terminated (110) surfaces with MA oriented along [110] or [111] directions. It is suggested that interface or substrate is necessary to stabilize various terminated surfaces of $MAPbI_3$.
ii) For tetragonal phase, the MA-I terminated (001) surface will not be stable with MA cations oriented along [001], although it is stable with MA along [110] and [111] directions.
iii) Interestingly, the electronic features can be tuned by the orientation of the MA cations, although it does not contribute to the band edge directly for the surfaces, much like the performance in the bulk system.

iv) Furthermore, we suggest experimentalists to adopt thin-film prepared under Pb-rich and I-rich conditions, which favors the stability of PbI_2-terminated (110) surfaces, as they have better hole transfer performance.

Acknowledgements

This work is financially supported by NSFC (Grant Nos. 11574088 and 51431001), the Foundation for Innovative Research Groups of the National Natural Science Foundation of China (Grant No. 51621001), and Natural Science Foundation of Guangdong Province of China (Grant No. 2016A030312011). The computer times at National Supercomputing Center in Guangzhou (NSCCGZ) are gratefully acknowledged.

Appendix A. Supporting information

Supporting information associated with this article can be found in the online version at doi:10.1016/j.jssc.2017.10.029.

References

[1] A. Kojima, K. Teshima, Y. Shirai, T. Miyasaka, J. Am. Chem. Soc. 131 (2009) 6050–6051.
[2] J.-H. Im, C.-R. Lee, J.-W. Lee, S.-W. Park, N.-G. Park, Nanoscale 3 (2011) 4088–4093.
[3] H.-S. Kim, C.-R. Lee, J.-H. Im, K.-B. Lee, T. Moehl, A. Marchioro, S.-J. Moon, R. Humphry-Baker, J.-H. Yum, J.E. Moser, M. Grätzel, N.-G. Park, Sci. Rep. 2 (2012) 591.
[4] I. Chung, B. Lee, J. He, R.P.H. Chang, M.G. Kanatzidis, Nature 485 (2012) 486–489.
[5] M.M. Lee, J. Teuscher, T. Miyasaka, T.N. Murakami, H.J. Snaith, Science 338 (2012) 643.
[6] J. Burschka, N. Pellet, S.-J. Moon, R. Humphry-Baker, P. Gao, M.K. Nazeeruddin, M. Gratzel, Nature 499 (2013) 316–319.
[7] M. Liu, M.B. Johnston, H.J. Snaith, Nature 501 (2013) 395–398.
[8] N.-G. Park, J. Phys. Chem. Lett. 4 (2013) 2423–2429.
[9] S.D. Stranks, G.E. Eperon, G. Grancini, C. Menelaou, M.J.P. Alcocer, T. Leijtens, L.M. Herz, A. Petrozza, H.J. Snaith, Science 342 (2013) 341.
[10] Q. Chen, H. Zhou, Z. Hong, S. Luo, H.-S. Duan, H.-H. Wang, Y. Liu, G. Li, Y. Yang, J. Am. Chem. Soc. 136 (2014) 622–625.
[11] D. Liu, T.L. Kelly, Nat. Photon. 8 (2014) 133–138.
[12] H. Zhou, Q. Chen, G. Li, S. Luo, T.-b. Song, H.-S. Duan, Z. Hong, J. You, Y. Liu, Y. Yang, Science 345 (2014) 542.
[13] W.S. Yang, J.H. Noh, N.J. Jeon, Y.C. Kim, S. Ryu, J. Seo, S.I. Seok, Science 348 (2015) 1234.
[14] N.J. Jeon, J.H. Noh, W.S. Yang, Y.C. Kim, S. Ryu, J. Seo, S.I. Seok, Nature 517 (2015) 476–480.
[15] M. Saliba, T. Matsui, J.-Y. Seo, K. Domanski, J.-P. Correa-Baena, M.K. Nazeeruddin, S.M. Zakeeruddin, W. Tress, A. Abate, A. Hagfeldt, M. Gratzel, Energy Environ. Sci. 9 (2016) 1989–1997.
[16] NERAL, 2016. ⟨http://www.nrel.gov/ncpv/images/efficiency⟩.
[17] M.A. Green, K. Emery, Y. Hishikawa, W. Warta, E.D. Dunlop, Prog. Photovolt. Res. Appl. 23 (2015) 1–9.
[18] G. Xing, N. Mathews, S. Sun, S.S. Lim, Y.M. Lam, M. Grätzel, S. Mhaisalkar, T.C. Sum, Science 342 (2013) 344.
[19] C. Wehrenfennig, G.E. Eperon, M.B. Johnston, H.J. Snaith, L.M. Herz, Adv. Mater. 26 (2014) 1584–1589.
[20] Q. Lin, A. Armin, R.C.R. Nagiri, P.L. Burn, P. Meredith, Nat. Photon. 9 (2015) 106–112.
[21] A. Miyata, A. Mitioglu, P. Plochocka, O. Portugall, J.T.-W. Wang, S.D. Stranks, H.J. Snaith, R.J. Nicholas, Nat. Phys. 11 (2015) 582–587.
[22] Q. Dong, Y. Fang, Y. Shao, P. Mulligan, J. Qiu, L. Cao, J. Huang, Science 347 (2015) 967.
[23] F. Deschler, M. Price, S. Pathak, L.E. Klintberg, D.-D. Jarausch, R. Higler, S. Hüttner, T. Leijtens, S.D. Stranks, H.J. Snaith, M. Atatüre, R.T. Phillips, R.H. Friend, J. Phys. Chem. Lett. 5 (2014) 1421–1426.
[24] D. Shi, V. Adinolfi, R. Comin, M. Yuan, E. Alarousu, A. Buin, Y. Chen, S. Hoogland, A. Rothenberger, K. Katsiev, Y. Losovyj, X. Zhang, P.A. Dowben, O.F. Mohammed, E.H. Sargent, O.M. Bakr, Science 347 (2015) 519.
[25] V.M. Goldschmidt, Naturwissenschaften 14 (1926) 477–485.
[26] C. Li, X. Lu, W. Ding, L. Feng, Y. Gao, Z. Guo, Acta Crystallogr. Sect. B 64 (2008) 702–707.
[27] G. Kieslich, S. Sun, A.K. Cheetham, Chem. Sci. 5 (2014) 4712–4715.
[28] C.C. Stoumpos, M.G. Kanatzidis, Acc. Chem. Res. 48 (2015) 2791–2802.
[29] J.M. Ball, M.M. Lee, A. Hey, H.J. Snaith, Energy Environ. Sci. 6 (2013) 1739–1743.
[30] G.E. Eperon, G.M. Paterno, R.J. Sutton, A. Zampetti, A.A. Haghighirad, F. Cacialli, H.J. Snaith, J. Mater. Chem. A 3 (2015) 19688–19695.
[31] L.Q. Phuong, Y. Yamada, M. Nagai, N. Maruyama, A. Wakamiya, Y. Kanemitsu, J. Phys. Chem. Lett. 7 (2016) 2316–2321.
[32] L. Etgar, P. Gao, Z. Xue, Q. Peng, A.K. Chandiran, B. Liu, M.K. Nazeeruddin, M. Grätzel, J. Am. Chem. Soc. 134 (2012) 17396–17399.
[33] N. Wang, K. Zhao, T. Ding, W. Liu, A.S. Ahmed, Z. Wang, M. Tian, X.W. Sun, Q. Zhang, Adv. Energy Mater. 7 (2017) 1700522.
[34] T. Baikie, N.S. Barrow, Y. Fang, P.J. Keenan, P.R. Slater, R.O. Piltz, M. Gutmann, S.G. Mhaisalkar, T.J. White, J. Mater. Chem. A 3 (2015) 9298–9307.
[35] A.M.A. Leguy, J.M. Frost, A.P. McMahon, V.G. Sakai, W. Kockelmann, C. Law, X. Li, F. Foglia, A. Walsh, B.C. O'Regan, J. Nelson, J.T. Cabral, P.R.F. Barnes, Nat. Commun. 6 (2015) 7124.
[36] M.A. Pérez-Osorio, R.L. Milot, M.R. Filip, J.B. Patel, L.M. Herz, M.B. Johnston, F. Giustino, J. Phys. Chem. C 119 (2015) 25703–25718.
[37] C. Motta, F. El-Mellouhi, S. Kais, N. Tabet, F. Alharbi, S. Sanvito, Nat. Commun. 6 (2015) 7026.
[38] G.R. Berdiyorov, A. Kachmar, F. El-Mellouhi, M.A. Carignano, M. El-Amine Madjet, J. Phys. Chem. C 120 (2016) 16259–16270.
[39] W. Geng, L. Zhang, Y.-N. Zhang, W.-M. Lau, L.-M. Liu, J. Phys. Chem. C 118 (2014) 19565–19571.
[40] B. Kang, K. Biswas, J. Phys. Chem. C 121 (2017) 8319–8326.
[41] J. Haruyama, K. Sodeyama, L. Han, Y. Tateyama, J. Phys. Chem. Lett. 5 (2014) 2903–2909.
[42] Y. Wang, B.G. Sumpter, J. Huang, H. Zhang, P. Liu, H. Yang, H. Zhao, J. Phys. Chem. C 119 (2015) 1136–1145.
[43] W. Geng, C.-J. Tong, Z.-K. Tang, C. Yam, Y.-N. Zhang, W.-M. Lau, L.-M. Liu, J. Materiomics, 1 (2015) 213–220.
[44] J. Haruyama, K. Sodeyama, L. Han, Y. Tateyama, Acc. Chem. Res. 49 (2016) 554–561.
[45] G. Kresse, J. Hafner, Phys. Rev. B 47 (1993) 558.
[46] G. Kresse, J. Furthmüller, Phys. Rev. B 54 (1996) 11169.
[47] P.E. Blöchl, Phys. Rev. B 50 (1994) 17953–17979.
[48] G. Kresse, D. Joubert, Phys. Rev. B 59 (1999) 1758–1775.
[49] J.P. Perdew, K. Burke, M. Ernzerhof, Phys. Rev. Lett. 77 (1996) 3865.
[50] J. Klimeš, D.R. Bowler, A. Michaelides, Phys. Rev. B 83 (2011) 195131.
[51] A. Poglitsch, D. Weber, J. Chem. Phys. 87 (1987) 6373–6378.
[52] N. Claudine, J. Phys.: Condens. Matter 12 (2000) R367.
[53] E. Heifets, J. Ho, B. Merinov, Phys. Rev. B 75 (2007) 155431.
[54] F. Bottin, F. Finocchi, C. Noguera, Phys. Rev. B 68 (2003) 035418.
[55] H. Chen, Y.-h. Ding, H.-t. Yu, Y. Xie, J. Phys. Chem. C 119 (2015) 9364–9374.
[56] X. Huang, T.R. Paudel, P.A. Dowben, S. Dong, E.Y. Tsymbal, Phys. Rev. B 94 (2016) 195309.
[57] S.B. Zhang, J.E. Northrup, Phys. Rev. Lett. 67 (1991) 2339–2342.
[58] Y. Kawamura, H. Mashiyama, K. Hasebe, J. Phys. Soc. Jpn. 71 (2002) 1694–1697.
[59] W.-J. Yin, T. Shi, Y. Yan, Appl. Phys. Lett. 104 (2014) 063903.
[60] W.-J. Yin, J.-H. Yang, J. Kang, Y. Yan, S.-H. Wei, J. Mater. Chem. A 3 (2015) 8926–8942.
[61] J. Qiu, Y. Qiu, K. Yan, M. Zhong, C. Mu, H. Yan, S. Yang, Nanoscale 5 (2013) 3245–3248.
[62] W.-J. Yin, T. Shi, Y. Yan, Adv. Mater. 26 (2014) 4653–4658.
[63] S.-H. Wei, A. Zunger, Phys. Rev. B 55 (1997) 13605–13610.
[64] D.A. Egger, L. Kronik, J. Phys. Chem. Lett. 5 (2014) 2728–2733.
[65] S. Bae, J.-S. Park, I.K. Han, T.J. Shin, W.H. Jo, Sol. Energy Mater. Sol. Cells 160 (2017) 77–84.
[66] Q. Liang, J. Liu, Z. Cheng, Y. Li, L. Chen, R. Zhang, J. Zhang, Y. Han, J. Mater. Chem. A 4 (2016) 223–232.
[67] M. Bouchard, J. Hilhorst, S. Pouget, F. Alam, M. Mendez, D. Djurado, D. Aldakov, T. Schülli, P. Reiss, J. Phys. Chem. C 121 (2017) 7596–7602.
[68] C. Grote, R.F. Berger, J. Phys. Chem. C 119 (2015) 22832–22837.
[69] Z. Xiao, W. Meng, J. Wang, D.B. Mitzi, Y. Yan, Mater. Horiz. 4 (2017) 206–216.
[70] I.C. Smith, E.T. Hoke, D. Solis-Ibarra, M.D. McGehee, H.I. Karunadasa, Angew. Chem. 126 (2014) 11414–11417.
[71] O. Selig, A. Sadhanala, C. Müller, R. Lovrincic, Z. Chen, Y.L.A. Rezus, J.M. Frost, T.L.C. Jansen, A.A. Bakulin, J. Am. Chem. Soc. 139 (2017) 4068–4074.
[72] D.J. Kubicki, D. Prochowicz, A. Hofstetter, P. Péchy, S.M. Zakeeruddin, M. Grätzel, L. Emsley, J. Am. Chem. Soc. 139 (2017) 10055–10061.